Journal of Fluids and Structures 125 (2024) 104076

Contents lists available at ScienceDirect

Journal of Fluids and Structures

journal homepage: www.elsevier.com/locate/jfs

# ADV measurements of blockage flow effects near a model jacket in waves and current

A.J. Archer [a,*], H.A. Wolgamot [a,b], J. Orszaghova [a,b], S. Dai [c], P.H. Taylor [a]

[a] Oceans Graduate School, University of Western Australia, WA 6009, Australia
[b] Marine Energy Research Australia, Great Southern Marine Research Facility, Albany, Western Australia, 6330, Australia
[c] Naval Architecture, Ocean and Marine Engineering Department, University of Strathclyde, Glasgow, United Kingdom

ARTICLE INFO

*Keywords:*
Offshore wind energy
Blockage
Acoustic doppler velocimeter
Wave–structure interactions
Actuator disc theory

ABSTRACT

Design standards for drag loading on offshore jacket structures do not presently account for the reduction in forces arising from flow blockage effects in the event of combined waves and current. This force reduction is believed to originate in reduced mean flow velocity through the jacket, but this has never been directly measured. To address this, we conducted physical-model tests which measured the flow adjacent to a jacket structure in combined waves and in-line currents using acoustic Doppler velocimeters. Results confirm a dramatic reduction in the mean flow velocity up-wave and down-wave of a model jacket in waves and current, far greater than the flow reduction observed in current alone. These results unambiguously confirm the significant additional blockage (and hence reduction in structural loads) not captured in current offshore design standards.

## 1. Introduction

Bottom founded jackets are commonly used to support offshore oil and gas platforms and, more recently, offshore wind turbines and electrical sub-stations. Jacket procurement cost is a major barrier to timely return on investment, hence efficient design is important. Despite the fact that hydrodynamic loading from waves and currents is a key input parameter to jacket design, this fluid loading behaviour is not fully understood even now. A Morison type calculation (Morison et al., 1950) has historically been used to estimate loads, where forces (mostly drag) on each structural member are estimated assuming the rest of the structure does not influence the flowfield. This assumption was challenged by Taylor (1991) who showed that, in the event of a steady current, the jacket acts as an obstacle array, reducing local fluid velocities and accompanying drag forces, a flow effect called 'simple current blockage'. The postulated reduction in local fluid velocities was validated using results from experimental current-only jacket model tests by Finnigan (1992) and from field measurements by Forristall (1996). 'Simple current blockage' was later adopted in the API offshore industry design code (API, 2000). It was later shown that the combined action of waves and an in-line current give an even greater blockage effect than current alone, and hence a greater reduction in drag forces. This 'wave–current blockage' effect was modelled analytically in Taylor et al. (2013) for regular wave-driven oscillatory flow and current, with the model showing good agreement with experimental force measurements of Allender and Petrauskas (1987). Wave–current blockage effects were also studied with experimental force measurements using forced oscillations of grids of perforated plates (Santo et al., 2014a,b) and later using regular and irregular waves incident on a 1:80 towed model jacket which was both rigidly supported (Santo et al., 2018a) and then allowed to dynamically respond (Santo et al., 2018b). All prior work on wave–current blockage has focused on

* Corresponding author.
*E-mail address:* aidan.archer@research.uwa.edu.au (A.J. Archer).

https://doi.org/10.1016/j.jfluidstructs.2024.104076
Received 19 October 2023; Received in revised form 21 December 2023; Accepted 10 January 2024
Available online 18 January 2024

forces, and either used computational fluid dynamics models or analytical models to estimate what the forces 'should' have been if these blockage effects were not present. While this force reduction effect is assumed to be caused by the reduction in the mean fluid velocity through the jacket, this has not yet been directly measured.

This paper aims to address this gap, and is essentially an extension of the prior work of Santo et al. (2018a,b). We tested the hypothesis that combined waves and in-line current will give a greater reduction in the mean fluid velocity through a jacket than the reduction in flow velocity from current alone. In line with the assumptions made in the analytical blockage model in Taylor et al. (2013), we hypothesised that there will be a small reduction in mean fluid velocity up-wave of the jacket associated with flow divergence around the jacket, and a much larger reduction in mean fluid velocity down-wave of the jacket associated with expansion of the wake. To this end, we analysed experimental measurements of flow velocities taken by two acoustic Doppler velocimeters, one positioned up-wave and the other positioned down-wave of a model jacket. We measured the flow effects using two different jackets, one with a densely-packed array of structural members representative of an oil and gas production platform, the other with a sparsely-packed array of structural members representative of a lightweight offshore wind jacket.

In this paper, we first recount the flow properties predicted by the simple current blockage model in Taylor (1991) (Section 2.1) and by the blockage model in Taylor et al. (2013) for combined current and wave-driven oscillatory flow (Section 2.2). Details of the experiment are given in Section 3 and scale effects are commented on in Section 3.1. Results and discussion are presented in three parts: current only tests (Section 4.1), regular waves and current tests (Section 4.2) and embedded focused wave groups and current tests (Section 4.3). We conclude the paper in Section 5.

## 2. Analytical blockage models

### 2.1. Simple current blockage

In a uniform incident flow, Taylor (1991) showed that the global drag force can be written as an adjustment to the standard Morison form, accounting for the reduction in the undisturbed free-stream current $u_c$ to a value $u_{cs}$ through the disc within the actuator disc model,

$$F = \frac{1}{2}\rho\, C_d\, A\, u_{cs}^2, \tag{1}$$

where

$$u_{cs} = u_c \left( \frac{1}{1 + \dfrac{C_d A}{4A_f}} \right), \tag{2}$$

$\rho$ is the fluid density, $C_d$ is the non-dimensional drag coefficient, $A$ is the summed solid area of all structural members normal to the incident flow (the hydrodynamic area), and $A_f$ is the frontal area bounding the entire structure. The associated wake velocity can be expressed as

$$u_{wake} = u_c \frac{\left(1 - \dfrac{C_d A}{4A_f}\right)}{\left(1 + \dfrac{C_d A}{4A_f}\right)} \tag{3}$$

Forristall (1996) validated this model with field data collected from the Bullwinkle platform in the Gulf of Mexico during strong current events generated by loop eddies shed off the Gulf Stream, and the method was subsequently adopted in the API offshore industry design code (API, 2000).

### 2.2. Combined current and oscillatory flow

Taylor et al. (2013) proposed that the inclusion of regular waves provides additional blockage over the simple steady current case. To treat the addition of this wave-driven oscillatory flow, they combined the cycle-averaged Morison force

$$\frac{F_{av}}{\frac{1}{2}\rho C_d A} = \frac{1}{2\pi}\int_0^{2\pi} (u_w \cos\phi + u_{cs})|u_w \cos\phi + u_{cs}|\, \mathrm{d}\phi, \tag{4}$$

with the expression from actuator disc theory in mean flow

$$F_{av} = 2A_f \rho\, u_{cs}(u_c - u_{cs}), \tag{5}$$

where $u_w$ is the oscillatory flow amplitude, $\phi$ is the oscillation phase angle, and $u_{cs}$ is the reduced mean flow at the disc. This approach relies on the assumption that the mean flow near the disc is dominated by the global wake structure.

To obtain $u_{cs}$, the integral in Eq. (4) is evaluated, and the resulting expression solved iteratively. Dense obstacle arrays or high hydrodynamic loading regimes yield an un-physical result where $u_{cs}/u_c < 0.5$ and the predicted wake velocity, $u_{wake} = 2u_{cs} - u_c$, is negative. To maintain a physically meaningful solution ($u_{wake} \geq 0$) and still resolve the full hydrodynamic loading, Taylor et al.

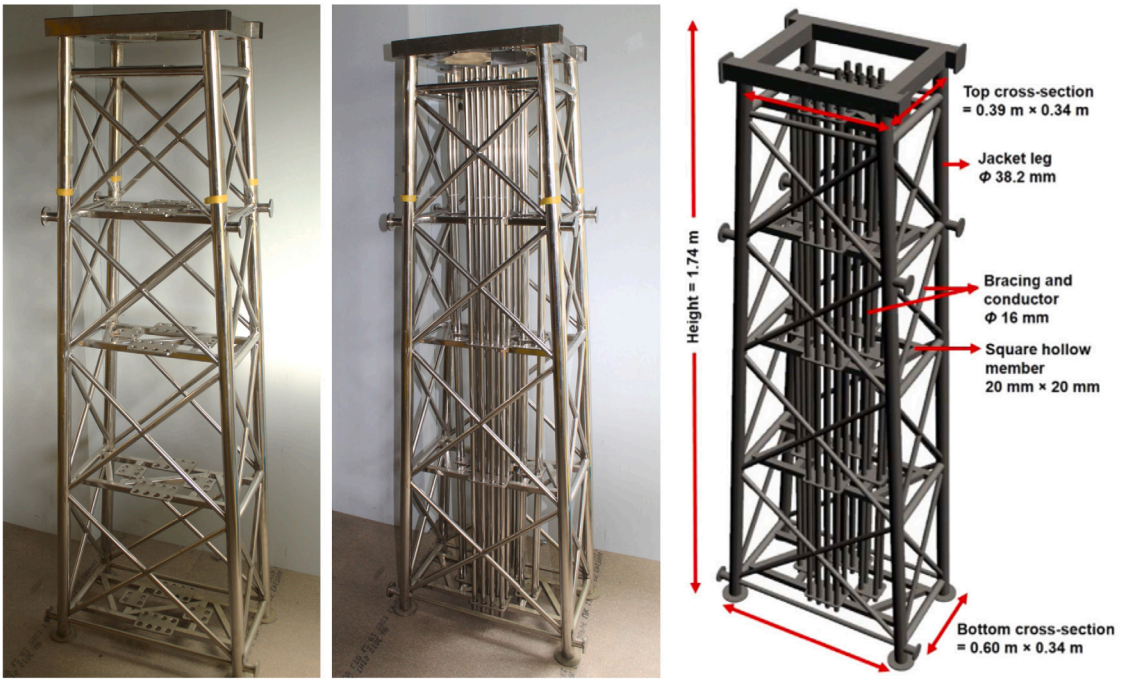


**Fig. 1.** Jacket models (left image shows sparse arrangement, middle image shows dense arrangement). Right image shows a 3D CAD model of the dense jacket annotated with relevant dimensions.

(2013) introduced the idea of splitting a single actuator disc into two. The first disc contains sufficient hydrodynamic area to reduce its wake speed to zero. The second disc, immersed in the stationary mean wake and containing the rest of the hydrodynamic area, then attracts only wave-induced oscillatory loading. Though an ad-hoc representation for the combined flowfield, they showed that the predicted forces were consistent with much previously published experimental data. This paper presents flow velocity measurements to assess the above ideas and enable development of design models that capture this wave–current blockage phenomena.

Recently, Cummins (2017) showed that the saturation of total hydrodynamic load for dense obstacle arrays in steady flow can be resolved without resorting to disc splitting by imposing geometric channel bounds. An extension of this approach to include the effect of regular waves is being developed by the authors.

## 3. Experimental setup

Experiments were conducted in the Kelvin Hydrodynamics Laboratory towing tank at the University of Strathclyde, Glasgow. The tank is 76 m long and 4.6 m wide with operating water depth of 1.8 m. Four Edinburgh Designs Ltd. hinged flap wavemakers with force-feedback control are located at one end, and a sloping beach acting as a passive absorber at the other end. A motorised carriage runs along the full length of the tank.

We tested the same jacket model used previously in Santo et al. (2018a,b), representative of a second generation North Sea platform (Fig. 1). The 1.74 m tall jacket consists of four cylindrical legs of 38.2 mm diameter, running parallel when viewed end-on but tapered when viewed broadside, giving a top and bottom cross-section of 0.39 m × 0.34 m and 0.60 m × 0.34 m respectively. 16 mm cylindrical members form diagonal bracing and vertical conductors, and 20 mm square tubing forms horizontal support frames. The 24 vertical conductors were removed and the tests repeated, allowing blockage investigation for a structure of lower hydrodynamic area, now more representative of a lightweight offshore wind jacket model. While in practice most offshore wind turbine jackets are triangular or square in plan, the hydrodynamic loading and flowfield behaviour tested here can be generalised to any jacket of comparable porosity. Henceforth, the jacket models with and without the conductor array will be referred to as the dense and sparse models respectively. The proposed scale of the models and the predicted scale effects are described in Section 3.1. Only the rectangular end-on jacket orientation was tested to elicit more blockage and reduce the effects of the tank walls.

The jacket was suspended from the carriage via a mounting frame with a double pendulum arrangement, leaving only the in-line horizontal force to be measured by a force transducer sampled at 137 Hz (Fig. 2). The jacket was submerged such that the distance from the jacket base to still water level was 1.33 m, leaving 0.47 m beneath the jacket base to the tank floor and 0.41 m above the still water level to the jacket top, ensuring the largest wave crests do not hit the mounting frame.

Water particle kinematics were measured by two Nortek Vectrino acoustic Doppler velocimeters (ADVs), one positioned 0.280 m from the jacket's front top horizontal cross-beam towards the wavemakers and one 0.448 m from the jacket's rear top horizontal

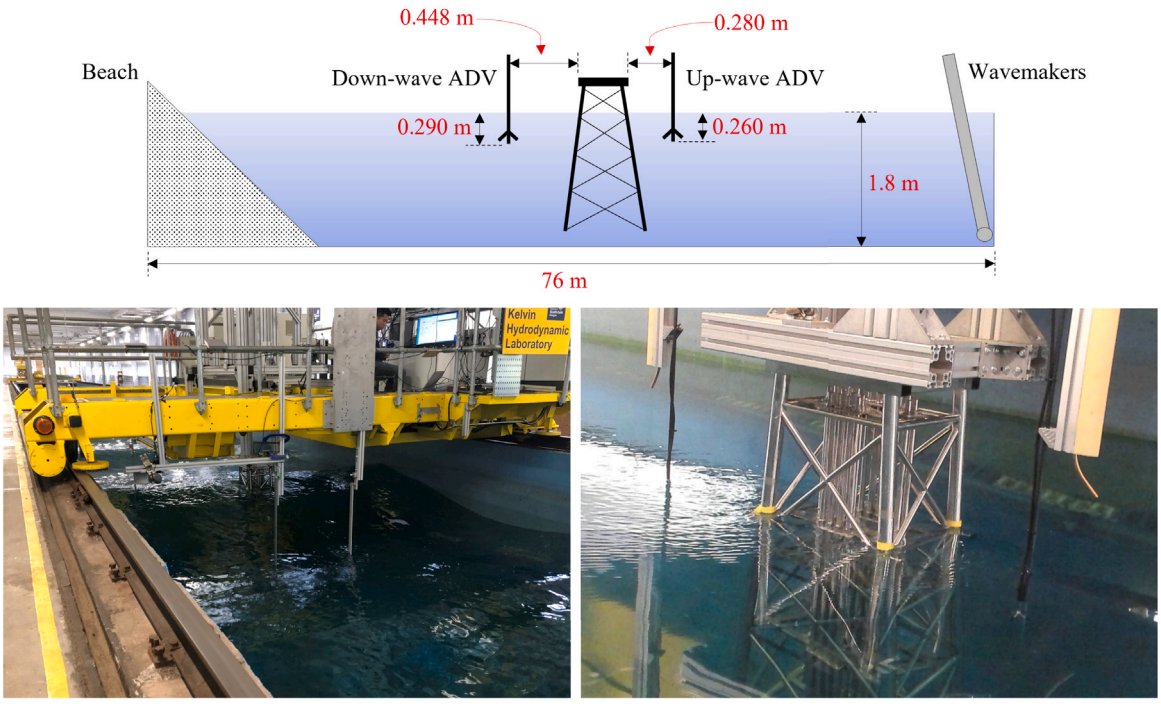


**Fig. 2.** Top panel shows a schematic of the towing tank with the position of both ADVs relative to the jacket (not to scale). Bottom left photograph shows the carriage with the jacket model suspended underneath when viewed in a down-wave direction. Bottom right photograph depicts a close-up of the jacket with the up-wave (to the right) and down-wave (to the left) ADVs installed.

cross-beam towards the beach. We wanted the ADVs to be positioned roughly 1 jacket-width away from the jacket as a compromise between competing flow effects: far enough from the model for the wake to expand and homogenise, and close enough to the model to minimise mixing between the wake and the bypass flow. In practice, the positions of the ADVs were determined by available mounting positions, but incidentally, the staggered arrangement allowed for an opportunity to measure the flow speeds at two different distances from the jacket. The ADVs' central transmitters were submerged 0.26 m and 0.29 m below still water level (such that they remain submerged under the largest wave trough, Fig. 2). Note that fluid velocities are sampled $\sim$ 50 mm below the transmitter. The ADVs were offset 5 mm laterally from the jacket and flume midline. For clarity, the ADVs will be referred to as up-wave and down-wave (relative to the jacket). Hollow glass microspheres, originally developed by 3M for use as a filler for composites, were used as seeding material. These glass particles are suspended in the tank and move at the same speed as the surrounding fluid, acting to passively reflect sound waves emitted from the ADV transducer (Nortek, 2018). The free surface at the jacket was sampled by a resistance-based wave probe mounted from the carriage between the jacket and the tank wall. Measurements were recorded at 137 Hz and then interpolated to 100 Hz.

Seven uniform current speeds $u_c$ of −0.56, −0.28, −0.14, 0, 0.14, 0.28 and 0.56 m/s were simulated by towing the model through otherwise still water, thus representing currents with a uniform depth profile. Positive incident current speed is defined in the same direction as incident wave propagation, corresponding to the carriage moving towards the wavemaker (through still water or through waves generated by the wavemaker). Hence, with a positive current this adds to the positive wave kinematics in a crest to increase drag loading.

A subset of positive current speeds were also tested in combination with waves (waves propagating in the same direction as the current). Two sets of regular waves, with amplitudes $a$ of 0.11 m and 0.2 m, were generated at the wavemaker with a frequency of 0.52 Hz. Focused wave groups with 0.075 m and 0.012 m crest amplitudes at focus were generated according to a JONSWAP power spectrum truncated at 1 Hz with a peak frequency of 0.52 Hz. Focused wave groups were also embedded within 0.041 m and 0.055 m amplitude regular wave backgrounds.

### 3.1. Model scale effects

The dense jacket is a reasonably faithful geometric representation of a second-generation North Sea platform, with both the framing pattern and the member diameters Froude-scaled down to a 1:80 lab scale. The submerged model depth of 1.33 m therefore scales to a full-scale jacket in 106 m water depth. For the sparse jacket, we chose a full-scale water depth of 60 m which is typical for an offshore wind jacket development, leading to a model scale of 1:45. The tested wave and current conditions are Froude-scaled

values of an extreme sea state. For example, at 1:80 scale, a 0.28 m/s current and a 0.2 m regular wave with a frequency of 0.52 Hz Froude scales to a 2.5 m/s current and a 16 m wave with 17 s period.

The effect of scaling on the measured flow behaviour may depend on the values of the Reynolds number, $\mathrm{Re} = ul/\nu$, and the Keulegen–Carpenter number, $\mathrm{KC} = u_w T/l$, where $u$ is the fluid velocity, $l$ is the diameter of a jacket member, $\nu$ is the kinematic fluid viscosity, $u_w$ is the amplitude of the wave-driven flow velocity and $T$ is the wave period. The tests were done at $\mathrm{Re} \approx 10^3 - 10^4$ and at $\mathrm{KC} \approx 10 - 20$. At full-scale, Reynolds numbers are of the order of $10^6 - 10^7$ and KC-numbers do not change. The structure of the small-scale wake behind each jacket member will change at full-scale — see for example Section 3.3 of Sumer and Fredsøe (2006) for the discussion of flow around individual cylinders (though we note that the complex jacket structure will make the small-scale wakes interact and therefore become complex and hard to predict). However, more importantly for blockage effects, the global wake of the jacket is driven by total momentum losses through the structure, not by shed vortices off each structural member, and these shed vortices should have mixed out by the time the flow reaches the ADV. Hence, we expect our tank measurements of flow blockage to approximately represent the full-scale behaviour.

## 4. Results and discussion

### 4.1. Blockage in current only

The accuracy of the ADV measurements was validated by comparing against carriage speeds when no jacket was present, for current speeds of 0.14 m/s and 0.28 m/s. Median flow measurements of both ADVs were within 2% of measured carriage speeds.

To estimate drag coefficients and interpret blockage measurements in current only, we use the simple current blockage model discussed in Section 2.1. The model collapses a structure into a single porous disc, hence does not apply to structures with members that are too densely-packed or structures which are long in the streamwise direction relative to their length across the flow direction (see Taylor et al. (2013)). Both the dense and sparse jackets comply with these assumptions as they are not structurally dense enough to cause the predicted wake speed to reverse in a uniform current (as explained in Section 2.2) and the ratio of their streamwise length to their length across the flow direction is representative of real jacket structures for which the model has been validated (Forristall, 1996).

Force time histories for steady tow tests without waves were used with Eq. (1) to estimate the drag coefficients of both the dense and sparse jacket models. The frontal area $A_f$ of both models is 0.55 $m^2$, while the hydrodynamic areas $A$ of the dense and sparse jackets are 1.12 and 0.54 $m^2$ respectively, with all areas measured to 0.25 m above still water level. Measured mean forces are plotted in Fig. 3(a, c). The linearity of the relationship between force and current-squared confirms the appropriateness of the Morison drag form used in simple current blockage (Eq. (1)). The $C_d$ values which give the best fit to the measured drag force are 0.70 for the dense jacket and 0.87 for the sparse jacket. These low drag coefficients can be interpreted by considering local shielding effects: structural members which trail behind leading members will experience reduced forces, hence they effectively have lower drag coefficients. The dense jacket with its tightly-packed conductor array has large local shielding effects, hence a lower drag coefficient. Semi-equivalently, the highly-blocked conductor array in the dense jacket can be modelled by adjusting the apportioning of hydrodynamic area across the actuator disc (Appendix B). By doing so, comparable drag coefficients between the dense and sparse jacket can be derived.

ADV measurements of the mean upstream and downstream fluid velocities are shown in Fig. 3(b, d). Note the two sets of measurements at each current speed formed by towing the model at positive and negative current speeds. The model is identical when viewed from each end, but the up-wave and down-wave ADVs are not symmetrically positioned relative to the centre of the jacket, hence the positive and negative tow directions give upstream and downstream flow velocity measurements at two different spatial points. The presence of the dense jacket acts to reduce both the upstream and downstream flow velocity below the free-stream velocity. The downstream flow velocity has good agreement with that predicted by Eq. (3) for the fully expanded wake when the model is towed in a positive tow direction, indicating the appropriateness of the estimated $C_d$. For measurements with the sparse jacket, upstream and downstream flow speeds are slightly reduced but to a much lower extent than with the dense jacket, with downstream velocities exceeding that predicted by Eq. (3). A clear limitation to the experiments is that the bulk flow behaviour can only be inferred from point measurements. The flow structure is likely to vary across the width of the sparse jacket, which has very little hydrodynamic area through its centre and most of the area concentrated on the outer perimeter when viewed from above.

The mean upstream and downstream flow speed measurements are lower when the model is towed in the positive direction (from beach to wavemakers) compared with the negative tow direction. A positive tow direction results in the upstream flow measurement closer to the jacket front, reading a stronger upstream divergence and thus reduced flow. We expect the upstream flow divergence ahead of the jacket to be localised to a short distance of the order of the frontal width of the jacket as this part of the flow is irrotational (see Fig. 3 in Santo et al. (2014a)). A positive tow direction also results in the downstream flow measurement being slightly further away from the jacket rear, closer to the fully relaxed wake region theorised by actuator disc models. Whether the ADVs are positioned in this fully relaxed wake is uncertain, partially because we did not collect enough spatial measurements to estimate this, and partially because the real wake behaviour is distorted by mixing of the wake with the bypass flow (which actuator disc theory ignores). So, comparisons between experimental flow measurements and theoretical predictions cannot be expected to show correspondence in every respect given the simplifications inherent in the analytical model. Nonetheless, we stress that to test our hypothesis, namely that waves and current give a greater reduction in the mean flow compared to current alone, it does not matter whether we measure the flow in the fully relaxed wake.

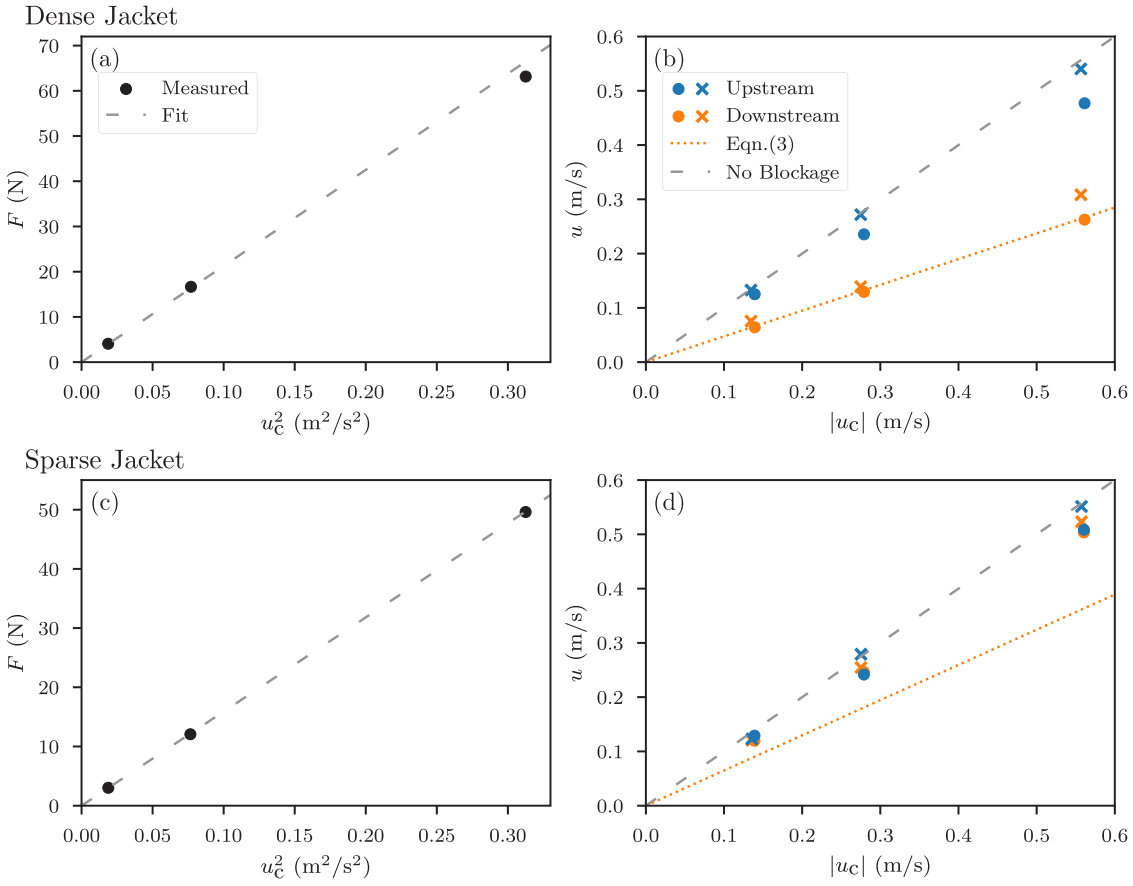


**Fig. 3.** Measured global force (a, c) and associated mean upstream and downstream horizontal flow velocities (b, d) for different steady current speeds $u_c$. Flow velocities measured in positive tow direction tests are indicated with • and those measured in negative tow direction tests indicated with ×.

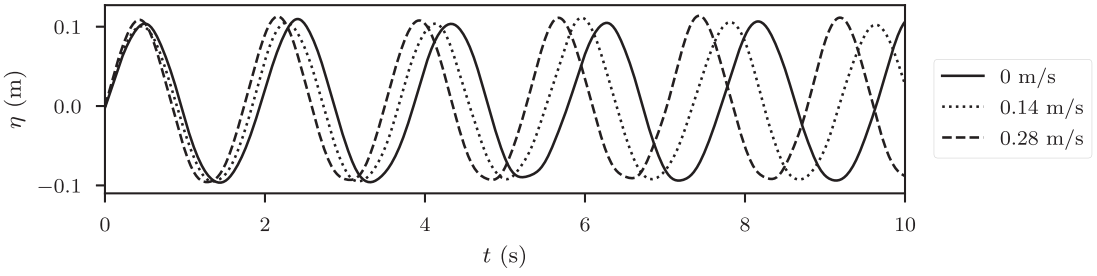


**Fig. 4.** Free surface timeseries of three regular waves ($a = 0.11$ m) with varying current speeds, as observed in the jacket's moving reference frame.

### 4.2. Blockage in combined regular waves and current

Towing the carriage towards the wavemaker to simulate combined wave and in-line current regimes acts to increase the encountered wave frequency due to the Doppler effect (Fig. 4). Importantly, wave kinematics are not modified. For clarity of comparisons between tests, subsequent figures will display horizontal time axes in a non-dimensional form, $t/T$, where $T$ is the regular wave period in a reference frame moving with the jacket.

Undisturbed wave kinematics at the up-wave and down-wave ADV depths were measured with the jacket model removed from the tank for regular waves of 0.11 m amplitude and 0.52 Hz frequency (giving a wave steepness $ka = 0.12$) whilst the carriage was held stationary. Fig. 5(a) compares the cycle-averaged horizontal velocity measurements to theory using a Stokes expansion to third order (Stokes, 1880). The linear free-surface amplitude and wave frequency used in the theoretical model are estimated from a fit to the measured free surface with the form given by Eq. (A.1), see Fig. 5(c). Measured oscillation amplitudes agree well with theory, but there appears to be a small mean flow of ~0.02 m/s backwards towards the wavemakers. While some uncertainty in

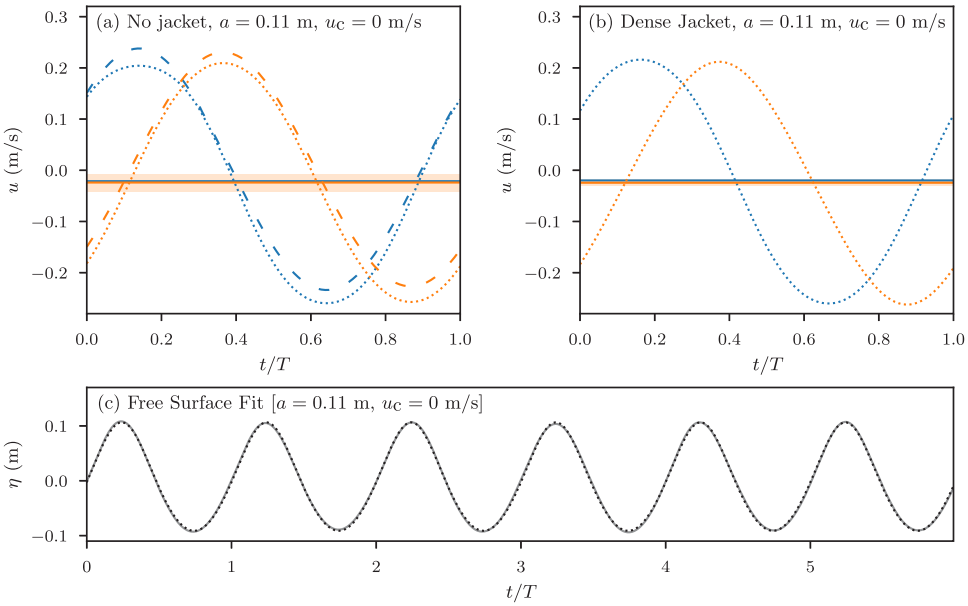


**Fig. 5.** a–b: Up-wave (····) and down-wave (····) horizontal ADV fluid velocity for regular waves with no current, ensemble averaged over multiple wave periods ($T$). Horizontal solid lines represent mean fluid velocities over a wave cycle, and the shaded horizontal bands represent the uncertainty ($\pm 1$ standard deviation) in this estimate. For (a), dashed lines represent theoretical fluid velocities as given by a Stokes expansion to third-order. c: Fit (····) to free surface (——) measured by a wave gauge out to the side of the carriage between ADVs for test conditions in (a).

the mean flow estimate exists, quantified by the standard deviation of the low-frequency (<0.3 Hz) signal component, this cannot fully account for the observed mean behaviour. This mean flow has no discernible trend over the 12 wave cycles used for averaging and is presumably the return flow underneath the regular wave train. Approximately half of the measured mean velocity can be accounted for if one assumes that the total return flow balancing the net volume flux driven by the theoretical Stokes drift is a uniform velocity over the water column.

Fluid velocities were again measured with the same regular wave train, now with the dense jacket installed between the up-wave and down-wave ADVs (Fig. 5(b)). No reduction in the up-wave or down-wave flow is seen compared to the case when no jacket was present. Hence, there is no evidence of any significant blockage for regular waves without current. This assumption was made in the analytical model by Taylor et al. (2013) and given experimental support by focused wave group tests of Santo et al. (2018a) where a larger value of $C_d$ was required to fit the force–time histories for waves alone compared to combined wave and current cases. By extension, Fig. 7 shows that the regular wave induced oscillatory flow component is unaltered by the presence of the jacket even with a steady current present.

We found that raw ADV data for combined regular wave and current tests had a high degree of data corruption and required significant post-processing to make it ready for use. This was in part due to signal noise linked to periods of poor seeding, and in part due to signal processing errors typified by large vertical steps in the data. Application of a data cleaning algorithm (presented in Appendix A), which relies on knowledge of the bulk flow behaviour, recovered much of the signal.

Repeat tests were conducted for two wave–current regimes, with the cycle-averaged cleaned ADV signals for each test presented in Fig. 6(d, e). The down-wave ADV root-mean-square error is below 0.02 m/s for both repeat tests, hence repeatability is satisfactory given we are interested in the bulk mean-flow behaviour.

The cleaned signals were averaged per wave cycle, with the cycle intervals determined from the free surface zero up-crossings measured by the wave probe adjacent to the jacket. Fig. 6 presents the cycle-averaged fluid velocity time-series for five test regimes for the two jacket models and a range of wave–current combinations, with the mean flow over this averaged cycle indicated by horizontal solid lines. For all regimes, the combination of waves and current gives a greater reduction in both the up-wave and down-wave mean flow when compared to the flow velocities observed for the same current speed with no waves. While a small part of this reduction is driven by a return flow underneath the regular wave train (~0.02 m/s for $a = 0.11$ m tests, ~0.03 m/s for $a = 0.2$ m tests), the magnitude of the mean flow reduction in combined wave and current tests far exceeds the estimated return flow. The extra reduction can only be a result of more blockage. This result is particularly striking for the sparse jacket, where passing current with no waves through the jacket results in very little flow reduction, but the addition of regular waves yields significant flow reduction. Remarkably, the down-wave mean flow nearly stops altogether for wave–current regimes (a), (c) and (e), a result theoretically predicted by actuator disc theory for combined current and oscillatory flow (Taylor et al., 2013) but never demonstrated in any previous physical experiments.

It is important to note that while the actual blocked mean flow within the jacket ($u_{cs}$ in Eq. (4)) was not measured due to practical constraints, the value of this blocked flow will lie between the measured mean up-wave and down-wave velocities.

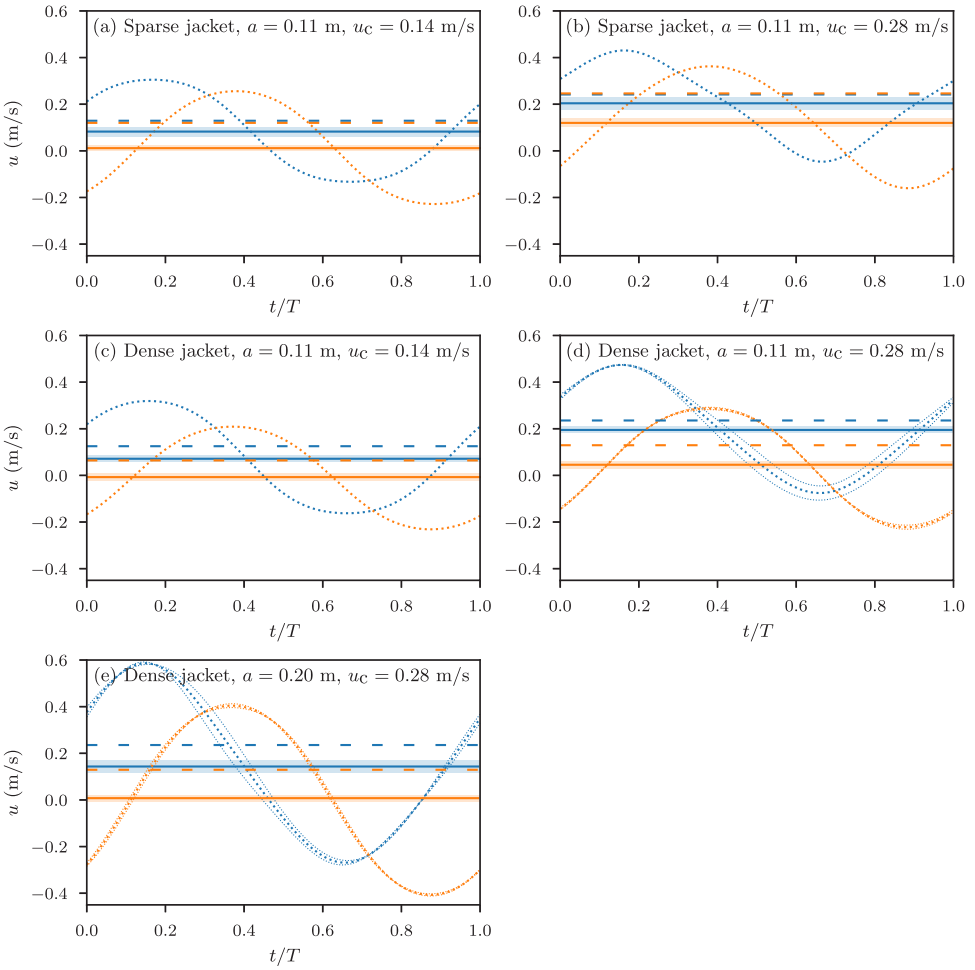


**Fig. 6.** Up-wave (····) and down-wave (····) horizontal ADV fluid velocity for different wave–current regimes, ensemble averaged over multiple wave periods ($T$). Thin dotted lines in (d, e) represent cycle-averaged fluid velocities for repeat tests. Horizontal solid lines represent mean fluid velocities over a wave cycle, and the shaded bands represent the uncertainty (±1 standard deviation) in this estimate. Horizontal dashed lines represent mean fluid velocities for the same current speed with no waves.

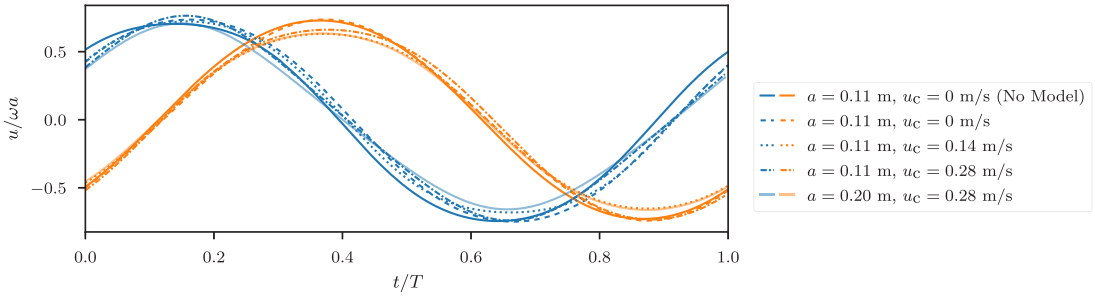


**Fig. 7.** Horizontal oscillatory component of up-wave (——) and down-wave (——) ADV fluid velocities, ensemble averaged over multiple wave periods ($T$), for the dense jacket subjected to varying regular wave and current regimes. The vertical velocity axis is given in non-dimensional terms, $\frac{u}{\omega a}$, where $\omega$ is the linear angular frequency and $a$ is the linear free surface amplitude. The mean flow in Fig. 6 has been removed for clarity.

To compare measured flow velocities to theory, it must be assumed that the down-wave ADV is far enough from the rear of the jacket such that it is in the fully-relaxed wake where mean fluid velocities are at a minimum. Peak wave velocities $u_w$ are estimated from the up-wave ADV oscillations for regular waves with no current. There is good agreement between theoretical and measured reductions in free-stream velocities $u_c$ in the wake of the jacket (Fig. 8). Of note, the mean flow (just) reverses for the dense jacket

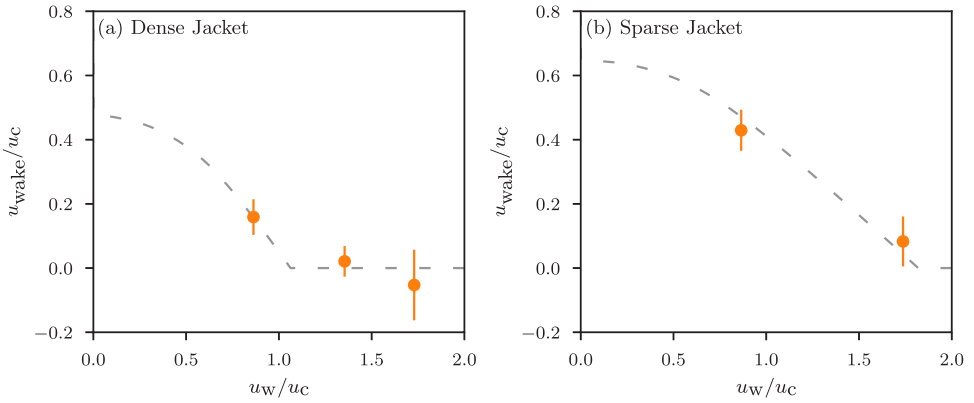


**Fig. 8.** Theoretical (– –) and measured (•) non-dimensionalised mean horizontal wake (down-wave) velocity versus peak wave velocity for the dense jacket (a) and sparse jacket (b). Error bars represent estimated standard deviation in mean down-wave ADV velocity.

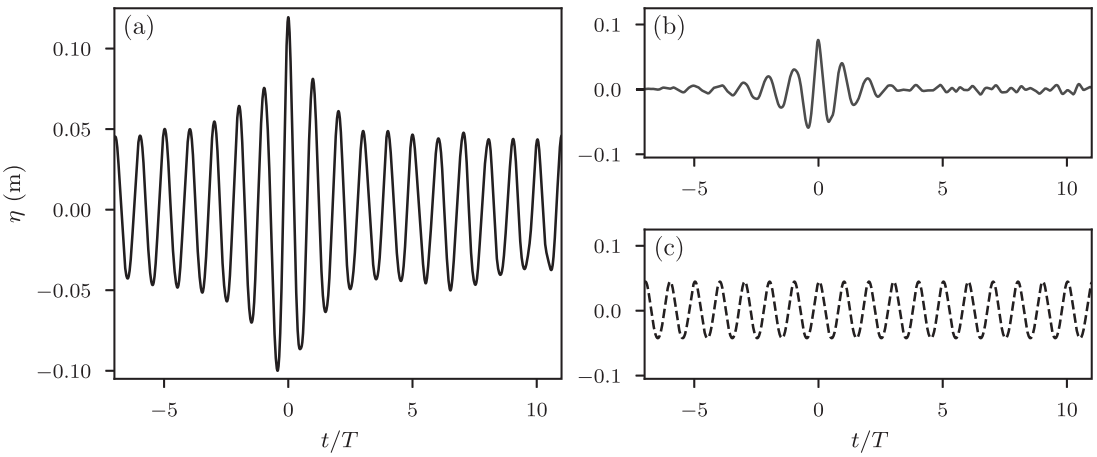


**Fig. 9.** Free surface measurements of an embedded focused wave group with $a_{\text{focused}}$ = 0.075 m and $a_{\text{regular}}$ = 0.041 m (a), separated by subtraction into its isolated focused wave group (b) and regular wave background (c) components. Horizontal time axis is normalised by the background regular wave period ($T$).

and for $u_w/u_c \approx 1.7$, which cannot be explained by this theory. The return flow measured under the regular wave trains, which has not been treated in the theoretical model, likely explains some of this behaviour. Uncertainty in the mean down-wave velocity estimate may also account for this result.

We emphasise that there are clear limitations in comparing this theory to experiments. Reducing the three-dimensional flow around a jacket in waves and current to a one-dimensional actuator disc model at a specified depth below still water neglects any vertical or lateral interactions and the effect of an oscillating free surface. Santo et al. (2017) numerically demonstrated substantial vertical flow interaction within a jacket for steady sheared current. In waves, the hyperbolic fluid velocity decay within the water column is likely to drive similar behaviour. On interpreting the experimental results, it is not known for certain whether the down-wave ADV is placed in the fully-relaxed wake. It is also not known how the flow behaviour varies transversely across the wake of the jacket and hence whether the bulk wake behaviour can be accurately inferred from a single point estimate. These limitations will be addressed with computational fluid dynamics modelling in future work.

### *4.3. Blockage in embedded focused wave groups and current*

While regular waves give the most extreme case of wave–current blockage when combined with an in-line current, they are a poor representation of the extreme sea states which offshore structures are designed to withstand. A focused wave group representing a large wave event embedded in a smaller regular wave background (Fig. 9) gives a more realistic design condition. The large crest represents an extreme wave and the regular background represent average waves in the sea-state. Fig. 10 shows up-wave and down-wave ADV signals from two embedded focused wave group tests with 0.28 m/s current.

The regular waves that make up the background signal are of much smaller amplitude than those used for pure regular wave tests. The additional blockage provided by this regular wave background is accordingly smaller: the up-wave ADV measures a mean flow

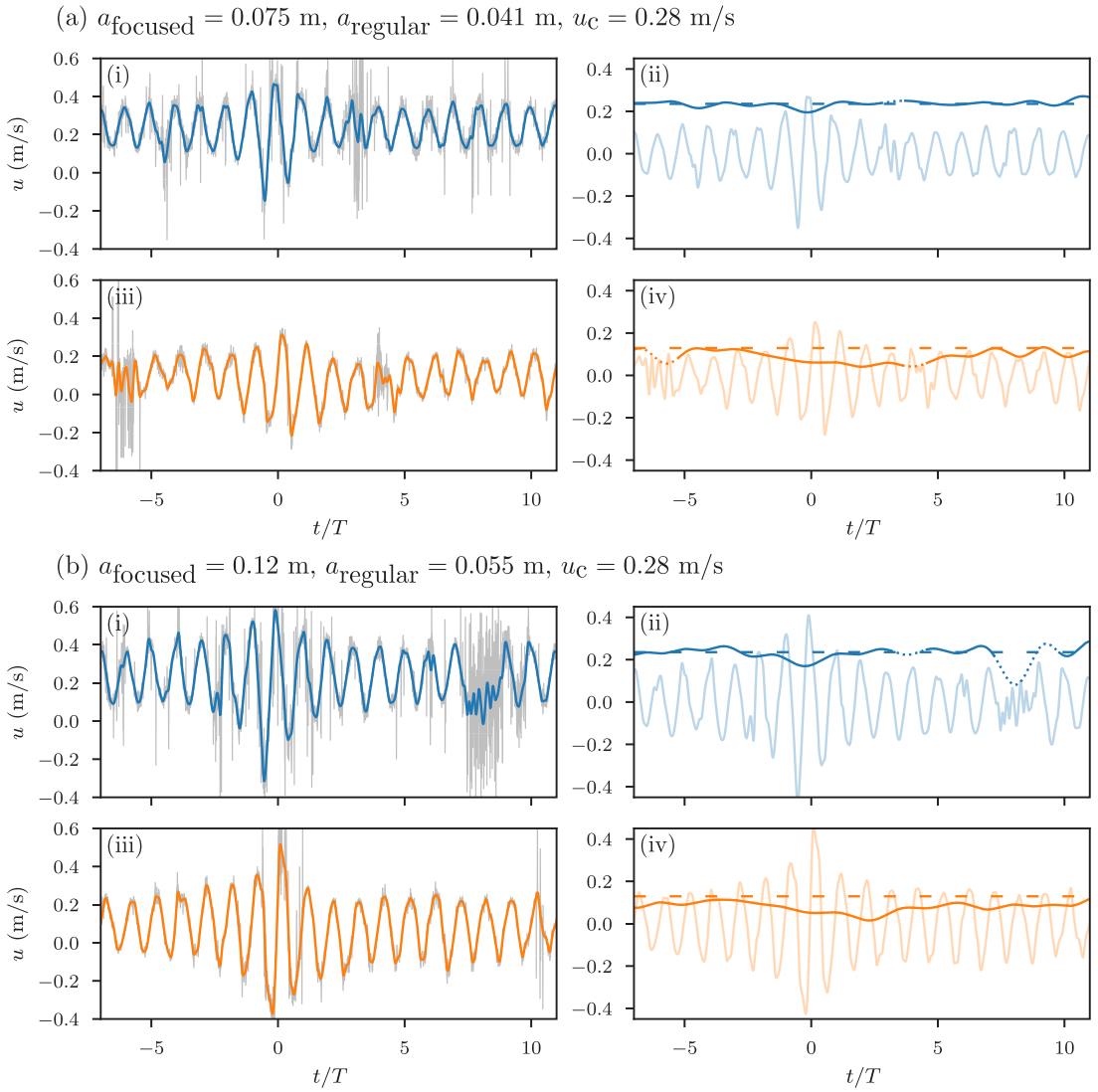


**Fig. 10.** Up-wave (—) and down-wave (—) horizontal ADV fluid velocities for embedded focused wave groups in regular wave background with current. Left-hand plots depict raw and filtered signals. Right-hand plots separate the filtered signals into low frequency (<0.3 Hz) (bold line) and higher frequency (faint line) components. Dotted-line periods in low frequency plots represent periods of poor data quality. Horizontal dashed lines represent the mean measured fluid velocity for the same current speed and no waves.

similar to that measured for the same current speed without waves, and the down-wave ADV measures slightly reduced velocities either side of the embedded focused wave group ($t/T < -3$ or $t/T > 7$).

With the advent of the focused wave group passing through the jacket, the up-wave ADV detects a transient reduction in mean flow. Estimates of the second-order return flow under the larger focused wave group suggest that this effect accounts for some of this reduction. The remainder must be a result of the upstream divergence associated with extra transient blockage.

Down-wave ADVs measure a larger reduction in mean flow, with the low frequency signal component dropping to approximately half of the pre-focused wave group value in Fig. 10(a)(iv) and almost reaching zero mean flow in Fig. 10(b)(iv). This behaviour can only be a result of the extra wave–current blockage driven by the larger focused wave group. The reduction in down-wave mean flow persists over a much longer time scale than that measured by the up-wave ADV. The down-wave flow reduction appears to commence 2 wave periods before the focused wave group peak passes through the jacket and lasts up to 4 wave periods after, equating to a total time of approximately 6 wave periods. Presumably, this area of reduced flow local to the jacket (associated with global vorticity) is then advected downstream by the current and the flow around the jacket returns to its pre-focused wave group behaviour.

These results imply that the extra blockage provided by waves on an underlying current is transient in nature and is most pronounced around large wave events. This extra blockage serves to reduce the loads experienced on jacket structures from large

wave events. The period of suppressed mean flow after the focused wave group passes through the jacket implies that for a set of large waves, the structural loads from subsequent waves after the first large wave has travelled through the jacket may be further reduced. As the flow within the jacket structure could not be measured for practical reasons in our tests, it can only be inferred from the up-wave and down-wave behaviour. Computational fluid dynamics modelling will address this limitation in future work.

## 5. Conclusion

This paper reports laboratory-scale experimental measurements of the flow behaviour around a model jacket when subject to a range of wave and current conditions. Two jacket models with differing hydrodynamic area are tested to represent variations in jacket design across the oil and gas and offshore wind industries. The presence of the jacket acts to cause divergence of the upstream flow and reduce the downstream flow when placed in a steady current, a result consistent with simple current blockage and considered in current design standards. Combining waves with a current acts to reduce the mean flow significantly below the already reduced steady current case. This effect is most pronounced for regular waves which give close to zero mean flow in the wake of the jacket in some test regimes, a result theoretically predicted by theory but not physically observed until now. Actuator disc theory developed for combined steady and oscillatory flow gives reasonable agreement with measured mean wake velocities. Results from larger focused wave groups embedded in a smaller regular wave background demonstrate that this extra wave–current blockage is transient in nature and localised around the largest waves when peak structural loads occur. Importantly, while the flow at the jacket was not explicitly measured, the up-wave and down-wave flow measurements unambiguously demonstrate the flow reduction and therefore the load reduction from wave–current blockage. This physical behaviour is not captured in current offshore design standards. The implications of this work are far-reaching — more favourable re-assessment of existing oil and gas platforms, and cost-savings for jackets used for economically marginal offshore wind developments.

## CRediT authorship contribution statement

**A.J. Archer:** Formal analysis, Validation, Visualization, Writing – original draft. **H.A. Wolgamot:** Conceptualization, Funding acquisition, Investigation, Methodology, Project administration, Supervision, Validation, Writing – review & editing. **J. Orszaghova:** Methodology, Supervision, Writing – review & editing. **S. Dai:** Investigation, Methodology, Resources. **P.H. Taylor:** Conceptualization, Methodology, Supervision, Writing – review & editing.

## Declaration of competing interest

The authors declare that they have no known competing financial interests or personal relationships that could have appeared to influence the work reported in this paper.

## Data availability

Data will be made available on request.

## Acknowledgements

The authors acknowledge support from the ARC ITRH for Transforming energy Infrastructure through Digital Engineering, Australia (TIDE, http://TIDE.edu.au) which is led by The University of Western Australia, delivered with The University of Wollongong and several other Australian and International research partners, and funded by the Australian Research Council, Australia, INPEX Operations Australia, Shell Australia, Woodside Energy, Australia, Fugro Australia Marine, Australia, Wood Group Kenny Australia, RPS Group, Australia, Bureau Veritas, Australia and Lloyd's Register Global Technology, Australia (Grant No. IH200100009). The authors are grateful to Mike Efthymiou and Peter Tromans for discussions which prompted the use of ADVs in this experimental campaign. We thank Harrif Santo of TCOMS for sharing his expertise from previous work. We are grateful to Guangwei Zhao and the technicians at Kelvin Hydrodynamics Laboratory for their assistance and expertise. A.J. Archer is supported by a Forrest Scholarship, Australia provided by the Forrest Research Foundation. H.A. Wolgamot is supported by an Australian Research Council, Australia (ARC) Early Career Fellowship (DE200101478). H.A. Wolgamot and J. Orszaghova acknowledge the Australian Research Council Linkage Project LP210100397, the Research Impact Grant from the University of Western Australia, Australia, and the Blue Economy Cooperative Research Centre, Australia CRC-20180101, established and supported under the Australian Government's Cooperative Research Centres Program.

## Appendix A. Signal processing of ADV data

The ADV measurements were corrupted by intermittent jumps in data (shifting the data up or down by $\pm 1$ m/s). Importantly, apparently meaningful data was still recorded during these jumps. Fig. 11(a) depicts these jumps in raw ADV data amidst an

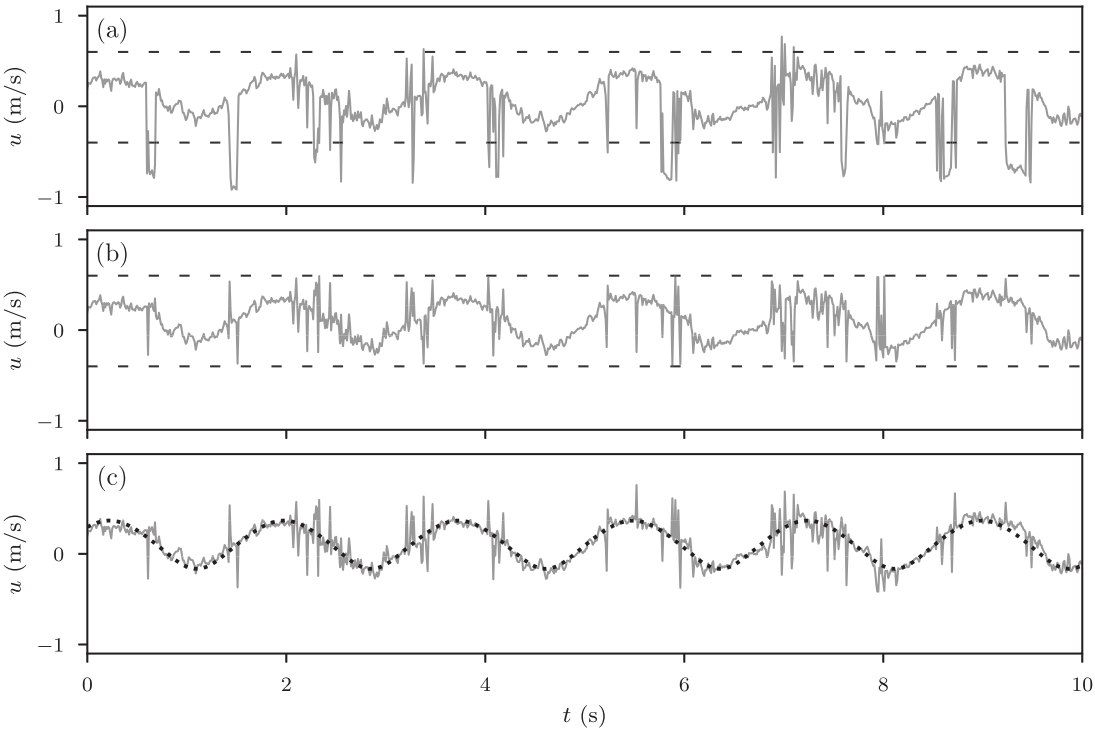


**Fig. 11.** 10 s excerpt of down-wave horizontal fluid measurements captured for a combined regular wave ($a$ = 0.11 m) and current ($u_c$ = 0.28 m/s) with the sparse jacket deployed. Raw data (a) is first cleaned by correcting data jumps with upper and lower bounds (b) and finally by curve fitting (c).

underlying oscillatory flow for a combined regular wave and current test. The source of these features is believed to be internal signal processing within the ADV software. This may be an artifact of insufficient seeding: the large volume of water in the KHL tank made it challenging to deliver consistent seeding. Aliasing in ADV beam velocities resulting from incorrectly configured velocity ranges may also explain this behaviour (Nortek, 2018).

While many ADV spike detection and replacement algorithms have been proposed (e.g., Otnes and Enochson, 1978; Goring and Nikora, 2002), here we describe a simple data cleaning method which makes use of the meaningful data recorded during the jumps. This method assumes that the flow is oscillatory and stationary over time, which holds true for regular waves and steady current.

Simple upper and lower bounds are imposed outside the range of the underlying sinusoidal flow (Fig. 11(b)). If the upper or lower bounds are exceeded, the signal is corrected by −1 or +1 m/s respectively. Fig. 11(b) depicts these bounds and their effect on correcting data jumps. While the bulk of the signal jumps have been corrected, some remain, and some have been over-corrected (e.g., $t \approx 8$ s). To clean these instances, the signal is low-pass filtered at 2 Hz and the unfiltered data is again corrected by −1 and +1 m/s if the difference between the unfiltered and filtered data exceeds respective +0.5 and −0.5 m/s thresholds.

The final cleaned signal (Fig. 11(c)) is low-pass filtered at 3 Hz and the result is fitted with a three-component cosine function consistent with the form given by a Stokes expansion to third order:

$$a_1 \cos(\omega t + \phi) + a_2 \cos(2\omega t + 2\phi) + a_3 \cos(3\omega t + 3\phi) + c, \tag{A.1}$$

where the peak angular frequency $\omega$ and time $t$ are treated as independent variables ($\omega$ is found by fitting the free surface with the same form as Eq. (A.1)) and other variables are fit using Python's lmfit package. Periods of data associated with poor seeding (e.g., $7 < t < 8$ s in Fig. 11(c)) are unrecoverable and are manually omitted from the data passed through the curve fit function.

Importantly, the underlying oscillatory component of the raw signal has not been altered during the data cleaning process. While some high frequency spikes remain in the cleaned data, their effect is largely nullified by low-pass filtering and curve fitting. The validity of this process relies on the fact that only the bulk (low frequency) flow behaviour is of relevance for blockage.

Note that ADV measurements for embedded focused wave groups are not oscillatory and hence curve fitting with the form given in Eq. (A.1) is not possible. The data cannot be further cleaned once data jumps are removed and the resulting signal is low-pass filtered at 3 Hz. Periods of bad data are unrecoverable and remain in the cleaned signal (Fig. 10) but the data quality around the focused wave group is of high enough quality to give insights into the bulk flow behaviour.

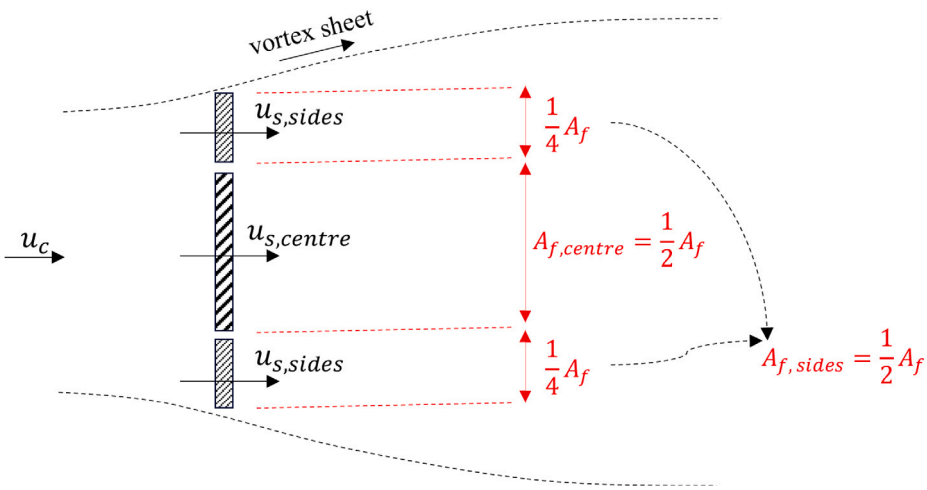


**Fig. 12.** Actuator disc model of dense jacket with non-uniform disc permeability.

## Appendix B. Actuator disc theory with non-uniform permeability

Typically, actuator disc models represent a porous structure as a uniformly-permeable disc. To model complex structures with variability in the density of hydrodynamic area across their frontal width, it may be appropriate to apportion an actuator disc into sections of different hydrodynamic area density. Actuator disc theory can then be applied to each disc section. This approach assumes negligible lateral interaction between the flow passing through each section (as has been assumed for actuator disc models in sheared flow; Draper et al., 2016).

The dense jacket can be represented by a combination of a central disc, which spans half the frontal area and contains half the hydrodynamic area of the sparse jacket plus the conductor array area, and two side discs which contain the remainder of both the frontal area and the sparse jacket's hydrodynamic area (Fig. 12). The exact disc apportionment is a decision made by the analyst based on the structural geometry.

Simple current blockage (Eq. (1)) is applied to each disc and summed to give the global force

$$\frac{F}{\frac{1}{2}\rho C_\mathrm{d}} = A_\mathrm{centre} u_{\mathrm{s,\ centre}}^2 + A_\mathrm{sides} u_{\mathrm{s,\ sides}}^2 \tag{B.1}$$

Substituting Eq. (2) gives

$$\frac{F}{\frac{1}{2}\rho C_\mathrm{d} u_\mathrm{c}^2} = A_\mathrm{centre}\left(\frac{1}{1+\frac{C_\mathrm{d}A_\mathrm{centre}}{4A_{\mathrm{f,\ centre}}}}\right)^2 + A_\mathrm{sides}\left(\frac{1}{1+\frac{C_\mathrm{d}A_\mathrm{sides}}{4A_{\mathrm{f,\ sides}}}}\right)^2, \tag{B.2}$$

and the expression is solved iteratively for $C_\mathrm{d}$ using the measured global force $F$.

## References


Allender, J., Petrauskas, C., 1987. Measured and predicted wave plus current loading on a laboratory-scale, space frame structure. In: Offshore Technology Conference. OTC5371, pp. 143–151.

API, 2000. API 2A-WSD: Recommended Practice for Planning, Designing and Constructing Fixed Offshore Platforms-Working Stress Design. American Petroleum Institute.

Cummins, P.F., 2017. Calibrating the loss coefficient of a porous plate. J. Waterw. Port Coast. Ocean Eng. 143 (2).

Draper, S., Nishino, T., Adcock, T.A.A., Taylor, P.H., 2016. Performance of an ideal turbine in an inviscid shear flow. J. Fluid Mech. 796, 86–112.

Finnigan, T.D., 1992. Current blockage effects on model-scale offshore platform. In: Civil Engineering in the Oceans V. ASCE, pp. 294–310.

Forristall, G.Z., 1996. Measurements of current blockage by the Bullwinkle platform. J. Atmos. Ocean. Technol. 13 (6), 1247–1266.

Goring, D.G., Nikora, V.I., 2002. Despiking acoustic doppler velocimeter data. J. Hydraul. Eng. 128 (1), 117–126.

Morison, J.R., O'Brien, M.P., Johnson, J.W., Schaaf, S.A., 1950. The force exerted by surface waves on piles. J. Pet. Technol. 2 (05), 149–154.

Nortek, 2018. The comprehensive manual for velocimeters. Available at https://www.nortekgroup.com/assets/software/N3015-030-Comprehensive-Manual-Velocimeters_1118.pdf.

Otnes, R.K., Enochson, L.D., 1978. Applied Time Series Analysis. Wiley, New York.

Santo, H., Stagonas, D., Buldakov, E., Taylor, P., 2017. Current blockage in sheared flow: Experiments and numerical modelling of regular waves and strongly sheared current through a space-frame structure. J. Fluids Struct. 70, 374–389.

Santo, H., Taylor, P.H., Bai, W., Choo, Y., 2014a. Blockage effects in wave and current: 2D planar simulations of combined regular oscillations and steady flow through porous blocks. Ocean Eng. 88, 174–186.

Santo, H., Taylor, P.H., Day, A., Nixon, E., Choo, Y., 2018a. Current blockage and extreme forces on a jacket model in focussed wave groups with current. J. Fluids Struct. 78, 24–35.
Santo, H., Taylor, P.H., Day, A., Nixon, E., Choo, Y., 2018b. Blockage and relative velocity Morison forces on a dynamically-responding jacket in large waves and current. J. Fluids Struct. 81, 161–178.
Santo, H., Taylor, P.H., Williamson, C., Choo, Y., 2014b. Current blockage experiments: force time histories on obstacle arrays in combined steady and oscillatory motion. J. Fluid Mech. 739, 143–178.
Stokes, G.G., 1880. Appendices and supplement to a paper on the theory of oscillation waves. Math. Phys. Pap. 1, 314–326.
Sumer, B.M., Fredsøe, J., 2006. Hydrodynamics Around Cylindrical Strucures, Revised ed. In: Number 26 in Advanced Series on Ocean Engineering, World Scientific Publishing, Singapore, OCLC: ocm76935393.
Taylor, P.H., 1991. Current blockage: reduced forces on offshore space-frame structures. In: Offshore Technology Conference. OTC 6519.
Taylor, P.H., Santo, H., Choo, Y., 2013. Current blockage: reduced Morison forces on space frame structures with high hydrodynamic area, and in regular waves and current. Ocean Eng. 57, 11–24.